Chinese Journal of Electronics
vol. 33, no. 5, pp. 1326–1336, September 2024
https://doi.org/10.23919/cje.2022.00.443

RESEARCH ARTICLE

An Algorithm of Deformation Image Correction Based on Spatial Mapping

Xiangyu DENG, Aijia ZHANG, and Jinhong YE

College of Physics and Electronic Engineering, Northwest Normal University, Lanzhou 730070, China

Corresponding author: Xiangyu DENG, Email: dengxy000@126.com
Manuscript Received January 30, 2023; Accepted August 7, 2023

Abstract — The original image undergoes geometric deformation in terms of position, shape, size, and orientation due to the shooting angle or capturing process during image acquisition. This leads to inconveniences and significant challenges in various image processing fields such as image fusion, denoising, recognition, and segmentation. To enhance the processing ability and recognition accuracy of deformation images, an adaptive algorithm for correcting image deformities is proposed for quadrilaterals and triangles. Firstly, the deformation image undergoes preprocessing, and the contour of the image edge is extracted. Then, discrete points on the image edge are identified to accurately locate the edges. Finally, the deformation of the quadrilateral or triangle is transformed into a standard rectangular or equilateral triangular image using the proposed three-dimensional homography transformation algorithm. This effectively completes the conversion from an irregular image to a regular image in an adaptive manner. Numerous experiments demonstrate that the proposed algorithm surpasses traditional methods like Hough transform and Radon transform. It improves the effectiveness of correcting deformation in images, effectively addresses the issue of geometric deformation, and provides a new technical method for processing deformation images.

Keywords — Image preprocessing, Image vertex positioning, Three-dimensional space, Homography transformation, Image correction.

Citation — Xiangyu DENG, Aijia ZHANG, and Jinhong YE, "An Algorithm of Deformation Image Correction Based on Spatial Mapping," *Chinese Journal of Electronics*, vol. 33, no. 5, pp. 1326–1336, 2024. doi: 10.23919/cje.2022.00.443.

I. Introduction

As the visual basis of human perception of the world, digital image [1], [2] is an important means for human to obtain, express and transmit information. At present, due to shooting angle or tilt angle (the angle between the imaging plane and the work-piece plane), hardware equipment [3], [4] and some uncontrollable factors in the acquisition of image information, the image has geometric deformation [5]–[7]. This causes the original regular object to appear as an arbitrary shape in the photo, which means the original image will have geometric deformation such as in geometric position, shape, size and orientation. For example, in the intelligent traffic system [8], due to the fixed angle and position of traffic cameras, most images of traffic signs have been obtained have varying degrees of tilt. This not only increases the complexity of the algorithm but also reduces the detection accuracy in the subsequent image processing, as well as bringing lots of inconveniences and challenges to the subsequent image fusion [9]–[11], image matching, image de-noising [12]–[14] and other image processing processes. Therefore, it is necessary to transform these deformation images with arbitrary shapes back to regular images, which play a unique role in target detection, intelligent driving, robot vision and other application fields [15],[16].

Correction of image deformation can be divided into large scene overall image correction [17] and small scene target image correction. In recent years, with the rapid development of image processing technology, many researchers around the world have carried out research on the whole image correction technology of large scene. For example, Lee [18] *et al.* proposed a distortion correction algorithm for estimating the cylindrical distortion parameters of fish-eye lens based on image quality by analyzing the characteristics of deformation image. Mao [19] *et al.* reconstructed the reverse mapping table online by

Associate Editor: Prof. Hongkai XIONG, Shanghai Jiao Tong University.

interpolation algorithm on FPGA and proposed a corrected algorithm of image distortion based on FPGA. Kirsten [20] *et al.* proposed an algorithm of MRI image distortion correction for low-field permanent magnet system with non-uniformity and gradient field nonlinear by combining image conjugate phase reconstruction, iteration and standard fast Fourier transform image reconstruction. Chen [21] *et al.* proposed a distortion correction algorithm for ultra-large field of view infrared images based on accurate model and inverse projection by using the inverse projection relationship between objects and images in imaging. Guan [22] *et al.* proposed a precision axial centering calibration technology by using the algorithm of optical lens axis to determine collimation. These algorithms provide a good idea for real-time image distortion correction.

In the research of small scene target image correction technology, the common algorithms for geometric distortion correction of target image include the Hough transform, the Radon transform and the affine transform, etc. Among them, Bafjaish [23] *et al.* proposed a script tilt detection and correction algorithm of Hough transform. The basic principle of the Hough transform is that transform the curves (including straight lines) in the image space into the parameter space, and determine the description parameters of the curve by detecting the extreme points in the parameter space, then extract regular curves in the image. Yu [24] *et al.* proposed an algorithm of automatic correction for track images based on Canny operator and Radon transform. The Radon transform is an integral transformation [25], which performs line integration of functions defined on a two-dimensional plane along any straight line on the plane. The algorithm of the Radon transform is a projection transformation actually, which realizes the image tilt correction through integral transformation. The traditional Hough transform and Radon transform are used to carry out a simple tilt correction, and the corrected image still has some geometric deformation, which does not solve the essential problem of geometric distortion of the image when using the Hough transform and the Radon transform to correct the deformed of the image. In addition, Li [26] *et al.* proposed a digital image correction algorithm based on the affine transformation. The affine transformation [27] has certain effects in image registration, image correction and texture correction, but the affine transformation only transforms the images into standard graphics, such as parallelogram and trapezoid transformation, which results in some limitations in the transformation of irregular quadrilateral. Javed *et al.* [28] proposed a recursive convolution neural network to realize the detection and recursive prediction correction of document corner points and finally realize the correction of documents. Yoo and Jun [29] proposed a license plate image correction algorithm based on deep angle prediction. Above two algorithms have high requirements on the amount of data and rely on a large number of data training. When the amount of data is insufficient, they will no longer be applicable. They are not suitable for scenes with large background interference and few available samples [30]–[32]. In view of the above problems, we propose an algorithm of spatial mapping transformation for predicting edge points. The proposed algorithm does not rely on mass data training and is universal to images in various fields. This algorithm can solve the geometric deformation problem in the process of image shooting, further improve the image processing ability of distorted graphics, and increase the accuracy of subsequent image matching and recognition.

The innovations of this paper are as follows:

1) In view of occluded images and incomplete edge segmentation images caused by light, we propose a vertex prediction method to find the vertex of the target image.

2) Based on the spatial mapping of quadrilateral target image, we propose a mapping method of triangular target image to realize the correction of triangular image.

3) By establishing a three-dimensional mathematical model, the matrix problem is transformed into a three-dimensional spatial geometry problem, and the mapping relationship is determined.

II. Image Correction Algorithm for Deformation

The flow chart of the proposed algorithm is shown in Figure 1.

Figure 1 Flow chart of algorithm.

1. Image preprocessing

Through a large number of experiments, it is found that the image will have a certain amount of shadow and noise due to the shooting light or mobile phone pixel problems. To solve these problem, the algorithm carries out adaptive filtering for binary image, filters out some unknown interference and noise, and then uses Canny [33], [34] algorithm to detect the edge of filtered image [35], and the mathematical morphology of the detected edge of the image expansion operation, used to thicken the image edge contour. The inflation will be “bigger”, the area of the target area will be merged with the background of the target area for the contact point to the target, after that the target boundary to expand outwards. Fill some voids in the target area and eliminate small particle noise contained in the target area. After the edge of the image is enhanced by mathematical morphology, the edge information of the image will be clearer. After the enhancement, all the connected domains of the image will be calculated, the smaller connected domains inside the image are filtered out, and the largest connected domain is retained, which means the edge of

the image will be retained. The image preprocessing process is shown in Figure 2.

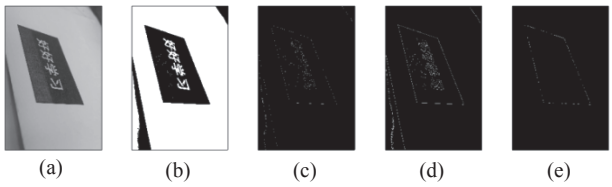

Figure 2 The process of image preprocessing. (a) Original image; (b) Result of adaptive filtering; (c) Result of image edge detection; (d) Result of mathematica molrphological expansion; (e) Maximum connected domain.

2. Image vertex positioning

As shown in Figure 3(a) the digital images are usually represented in the form of matrix, two-dimensional arrays are used to store image data in computer digital image processing programs. The pixel data of grayscale image is a matrix, the rows of the matrix correspond to the height of the image, the columns of the matrix correspond to the width of the image, the elements of the matrix correspond to the pixels of the image, and the value of the matrix elements is the gray value of the pixel. Therefore, it is necessary to use matrix theory and matrix algorithm to analyze and process digital images. Firstly, the data information of the image to be corrected and is the spatial geometric coordinate system. After the matrix is flipped and transposed, the two-dimensional matrix of the original image information can be transformed into a plane in the three-dimensional space.

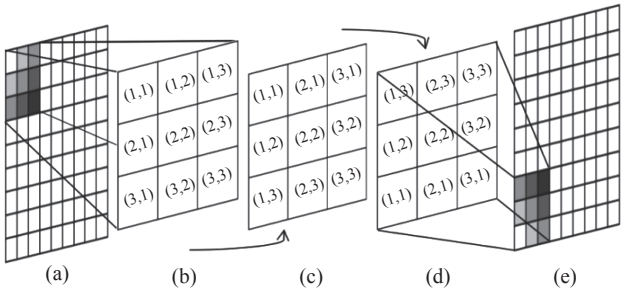

Figure 3 Convert the matrix to a rectangular coordinate system.

Figure 3(a) represents the pixel in the original image, and the value of the pixel is stored in the matrix. Figure 3(b) represents the position in the matrix where the value of each pixel is located. Transpose the matrix in Figure 3(b) to get the matrix in Figure 3(c), and then flip the matrix in Figure 3(d) to get the matrix in Figure 3(d). At this time, the position of the pixel in the matrix can correspond to the position in the rectangular coordinate system.

In the process of image homography transformation, the most important step is to find the vertex coordinates of the image and make homography relationship with the vertex coordinates. During the above processing of the image, due to the contrast of different images, or shooting angle different, it is not guaranteed that each image can be accurately segmented into a complete image edge and image vertex during image processing, as shown in Figure 4. Therefore, it is necessary to predict the edges and vertices of the image.

(a) Original image (b) Edge detection for vertex missing

Figure 4 Image edge detection.

In the proposed algorithm, the algorithm of least squares method and linear fitting is used to fit the line of image edge, so as to avoid the under-fitting and over-fitting in the single fitting. And find any two or three vertices of the image, and then use the found vertices to predict the last vertex to determine the image vertex by looking for the intersection of two straight lines.

1) Linear fitting

Linear fitting is to use straight lines to describe the functional relations between coordinates represented by discrete points. Linear fitting approximates discrete data by analytic expression in numerical analysis. In practice, discrete point sets or data are often multiple observation values or experimental values related to various physical problems and statistical problems. They are scattered, not only inconvenient to process, cannot accurately and fully reflect their inherent laws, but vulnerable to the influence of interference points. In order to eliminate this effect, the proposed algorithm adopted is the principle of random sample consensus (RANSAC) to get a more accurate fitting line. The result of linear fitting and the principle of RANSAC is shown in Figure 5.

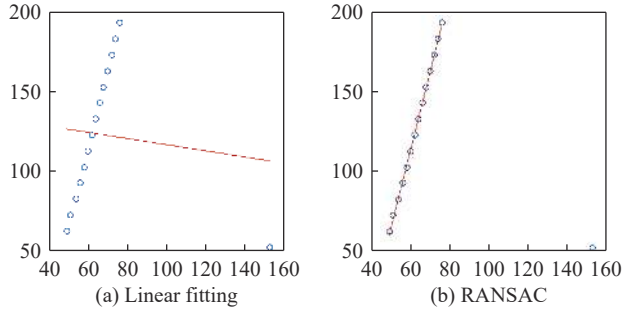

Figure 5 Comparison of linear fitting and RANSAC (arb. unit).

Figure 5 shows that linear fitting of discrete points filtered out by the method of RANSAC can well avoid interference of other discrete points connected with edge connected domain due to incomplete adaptive filtering in the image, resulting in over-fitting or under-fitting in the fitting process.

Figure 6 shows that the fitting of incomplete edges of Figure 4 after image preprocessing.

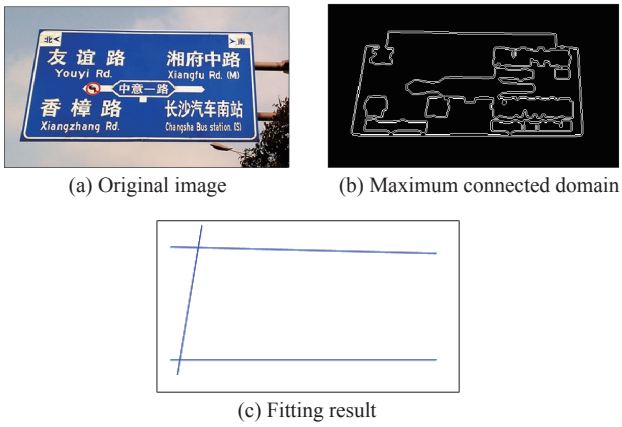

(a) Original image (b) Maximum connected domain

(c) Fitting result

Figure 6 The result of line fitting in Figure 4.

As shown in Figure 6(b), the image edges extracted after preprocessing are not necessarily complete image edge contours, so line segments need to be fitted to judge the four accurate vertices of the quadrilateral image, and the result of line fitting is shown in Figure 6(c).

2) Vertex prediction

Due to differences in lighting, shading, or other interfering factors, the edge contour of the image cannot be accurately or clearly extracted during the process of image preprocessing. A method of multiple gradient descent is proposed in this paper to predict the last vertex. Since a gradient descent method may not be able to find the global optimal solution, yet may be a local optimal solution, the local optimal solution found by the first GDA (gradient descent algorithm) method is trained again by GDA, and iterative processing is conducted until the optimal solution is found. In this process, a certain vertex is used as a ray endpoint to extend the ray. In the process of ray selection and rotation, it is necessary that judge the vertices obtained by fitting and ray vertices, and get the position of predicted points roughly. Then determine the direction of rotation of the rays. In the process of ray rotation, the number of the gray value is 1 in the image of the ray is taken as the objective function of the gradient descent method. The iteration of the gradient descent method is completed when the maximum number of the gray value is 1 in the image of the ray is found, which is close to the maximum value of the function. After vertex prediction, the image contour can be clearly drawn and the coordinate position of the image vertex can be found. The contour prediction of image is shown in Figure 7.

3. The relation of homography in three-dimensional space

After getting the vertices of the image, we can find the mapping relationship between the vertices of the irregular quadrilateral image and the vertices of the rectangular image, and the homography relationship between the vertices of the irregular triangle image and the vertices of the regular triangle. Due to the homography

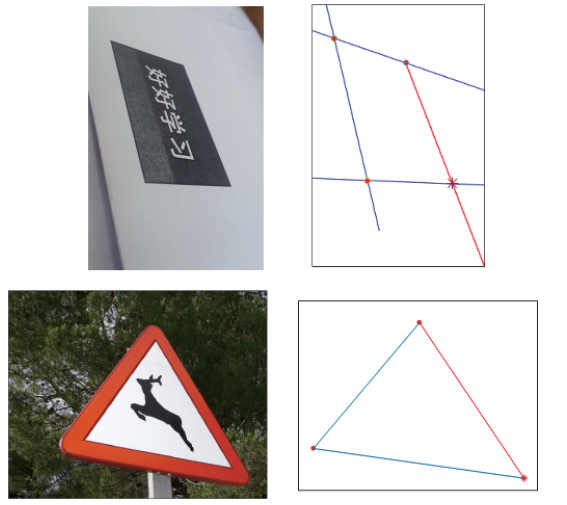

(a) Original image (b) The result of vertex prediction

Figure 7 Edge detection and contour prediction of image.

of quadrilateral and triangle is different, it is divided into two parts.

1) The relation of homography in quadrilateral

The mapping relationship of quadrilateral images in three-dimensional space is shown in Figure 8. Point E is the mapping point, namely the light source point. a_1–a_4 are the four vertices of the quadrilateral to be corrected; r_1–r_4 are the four vertices of the corrected rectangle.

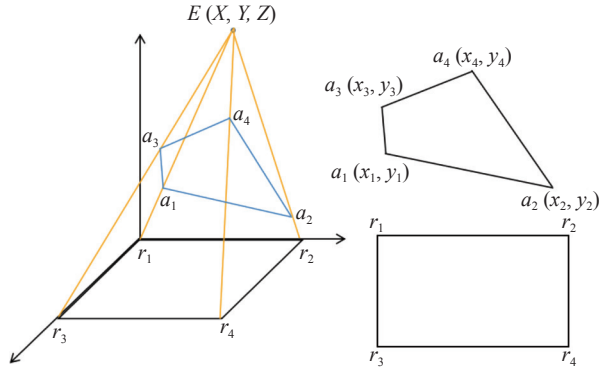

Figure 8 Mapping principle of quadrilateral image in three-dimensional space.

The linear relationship between vertices in Figure 8 is transformed into vector form. In an irregular quadrilateral, there are three linear vectors $\boldsymbol{a}_{12}$, $\boldsymbol{a}_{13}$ and $\boldsymbol{a}_{14}$, as well as all three vectors are on the same plane, which means any one of them can be expressed as a linear combination of the other two. The linear relationship between the three vectors is shown in (1). Picking any point a_0 in the quadrilateral irregularly, there exists a vector $\boldsymbol{a}_{10}$, which has the same linear relationship with vectors $\boldsymbol{a}_{12}$ and $\boldsymbol{a}_{13}$, as shown in (2). In the regular quadrilateral, there is any point r_0 and the vector is obtained $\boldsymbol{r}_{10}$, $\boldsymbol{r}_{12}$ and $\boldsymbol{r}_{13}$, then the linear relationship is shown in (3). According to (1)–(3), the corresponding relationship between point r_0 and point a_0 can be obtained

shown in (4). Equation (5) is obtained by inverse transformation of (4), and the mapping relationship between any point in the irregular quadrilateral and the standard rectangle can be obtained by substituting (5) into (2).

$$\boldsymbol{a}_{14} = u_0\boldsymbol{a}_{12} + u_1\boldsymbol{a}_{13} \tag{1}$$

$$\boldsymbol{a}_{10} = v_0\boldsymbol{a}_{12} + v_1\boldsymbol{a}_{13} \tag{2}$$

$$\boldsymbol{r}_{10} = w_0\boldsymbol{r}_{12} + w_1\boldsymbol{r}_{13} \tag{3}$$

$$(w_0, w_1) = \frac{(u_0 v_0, u_1 v_1)}{(u_0 + u_1 - 1) + (1 - u_1)\, v_0 + (1 - u_0)\, v_1} \tag{4}$$

$$(v_0, v_1) = \frac{(u_1 (u_0 + u_1 - 1)\, w_0, u_0 (u_0 + u_1 - 1)\, w_1)}{u_0 u_1 + u_1 (u_1 - 1)\, w_0 + u_0 (u_0 - 1)\, w_1} \tag{5}$$

where u_0, u_1, v_0, v_1, w_0, and w_1 respectively represents linear relationships of three coplanar vectors. Equations (1)–(5) can accomplish such a function: If we need to find a point in the rectangle corresponding to any point in the quadrilateral, we can find the corresponding value of the points u_0 and u_1, and then through the formula to find the value of w_0 and w_1, then use the values of w_0, w_1 and three vectors on the same plane, we can find the coordinates of a specific point in any quadrilateral. By iterating on the above steps several times, the entire irregular quadrilateral can be mapped to the standard rectangle.

2) The homography in the triangle

Different from the quadrilateral image, there is no condition for extracting three vectors from the same point to other vertices in the triangle image. As a result, the similar process for subsequent projections of the quadrilateral image cannot be completed. Therefore, we propose a new mapping relationship to correct the triangle image. The mapping relationship of triangular images in three-dimensional space is shown in Figure 9. Point E is the mapping point, named as the light source point. a_1–a_3 are the three vertices of the triangle to be corrected; r_1–r_3 are the three vertices of the corrected regular triangle.

The linear relationship between the vertices in Figure 9 is converted into a three-dimensional spatial geometric relationship, and the spatial plane equation of the triangle image to be corrected in the geometric coordinate system is shown in (6)–(10).

$$A = (y_2 - y_1) \times (z_3 - z_1) - (z_2 - z_1) \times (y_3 - y_1) \tag{6}$$

$$B = (x_3 - x_1) \times (z_2 - z_1) - (z_3 - z_1) \times (x_2 - x_1) \tag{7}$$

$$C = (x_2 - x_1) \times (y_3 - y_1) - (y_2 - y_1) \times (x_3 - x_1) \tag{8}$$

$$D = -(A \times x_1 + B \times y_1 + C \times z_1) \tag{9}$$

$$A \times x + B \times y + C \times z + D = 0 \tag{10}$$

where A, B, C and D respectively represent the intercepts of the plane equation; x_1, x_2, x_3, y_1, y_2, y_3, z_1, z_2 and z_3 respectively represent the coordinates of the three vertices of an irregular triangle.

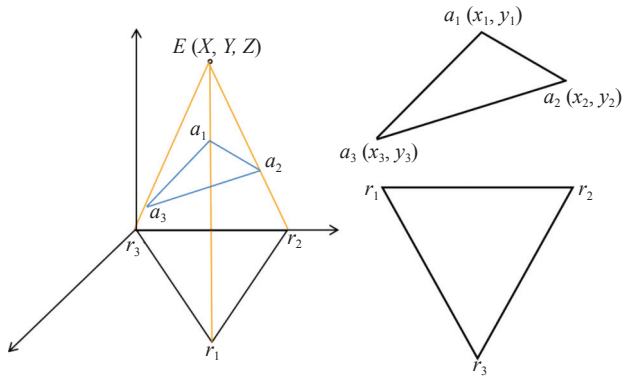

Figure 9 Mapping principle of triangular image in three-dimensional space.

In spatial geometry, three straight lines may not have only one intersection point, so one point of the irregular triangle is placed in the regular triangle, and then the vertex point E can be obtained, as shown in equations (11)–(13).

$$X = \frac{\left(\frac{\sqrt{3}}{2} \times l \times y_2\right) \times \left(y_1 - \frac{l}{2}\right) - y_2 \times \left(x_1 - \frac{\sqrt{3}}{2} \times l\right)}{x_2 \times \left(y_1 - \frac{l}{2}\right) - y_2 \times \left(x_1 - \frac{\sqrt{3}}{2} \times l\right)} \times y \times x_1 \tag{11}$$

$$Y = \frac{\left(\frac{\sqrt{3}}{2} \times l \times y_2\right) \times \left(y_1 - \frac{l}{2}\right) - y_2 \times \left(x_1 - \frac{\sqrt{3}}{2} \times l\right)}{x_2 \times \left(y_1 - \frac{l}{2}\right) - y_2 \times \left(x_1 - \frac{\sqrt{3}}{2} \times l\right)} \times y_2 \times y_1 \tag{12}$$

$$Z = \frac{\left(\frac{\sqrt{3}}{2} \times l \times y_2\right) \times \left(y_1 - \frac{l}{2}\right) - y_2 \times \left(x_1 - \frac{\sqrt{3}}{2} \times l\right)}{x_2 \times \left(y_1 - \frac{l}{2}\right) - y_2 \times \left(x_1 - \frac{\sqrt{3}}{2} \times l\right)} \times y_2 \times z_1 \tag{13}$$

where l represents the side length of the equilateral triangle after correction; X, Y and Z respectively represent the three-dimensional coordinates of point E. x_1, x_2, y_1, y_2, z_1 and z_2 respectively represent the coordinates of any two vertices of an irregular triangle.

A space straight line can be obtained by connecting any point $(x_{0i},\ y_{0i},\ z_{0i})$ in the standard regular triangle

with point E, as shown in (14).

$$\frac{x - x_{0i}}{X - x_{0i}} = \frac{y - y_{0i}}{Y - y_{0i}} = \frac{z - z_{0i}}{Z - z_{0i}} \tag{14}$$

The space straight line intersects the irregular plane at a point (x_{1i}, y_{1i}, z_{1i}), that is the reflection point (x_{0i}, y_{0i}, z_{0i}) in three-dimensional space, as shown in (15)–(17).

$$x_{1i} = \frac{(-D - B \times y_{0i}) \times (X - x_{0i}) + B \times (Y - y_{0i}) \times x_{0i} + C \times Z \times x_{0i}}{A \times (X - x_{0i}) + (Y - y_{0i}) + C \times Z} \tag{15}$$

$$y_{1i} = \frac{(-D - A \times x_{0i}) \times (Y - y_{0i}) + A \times (X - x_{0i}) \times y_{0i} + C \times Z \times y_{0i}}{A \times (X - x_{0i}) + (Y - y_{0i}) + C \times Z} \tag{16}$$

$$z_{1i} = \frac{(-D - A \times x_{0i} - B \times y_{0i}) \times Z}{A \times (X - x_{0i}) + (Y - y_{0i}) + C \times Z} \tag{17}$$

The whole irregular triangle can be mapped to the standard regular triangle by several iterations of the above steps for finding the reflection point of each point in the regular triangle.

III. Experimental Results and Analysis

1. Experimental results

The shooting images of Figure 10(a) are respectively corrected by Hough and Randon, The correction results are respectively shown in Figures 10(b) and (c). They reveal the two methods of correction only correct the tilt of the image, and the correction result is not satisfactory. Figure 10(d) is the correction result of the proposed algorithm for Figure 10(a), and the result of correction is better than those of Hough and Randon.

(a) (b) (c) (d)

Figure 10 Comparison of correction results. (a) Shooting image; (b) The result of Hough; (c) The result of Radon; (d) The result of the proposed algorithm.

Figures 10(b) and (c) demonstrate the application of Hough and Randon algorithms, where the image is geometrically rotated based on an edge as the reference. However, it should be noted that these methods do not effectively address the fundamental issue of image distortion. Figure 10(d) is the result of distortion correction by using the proposed algorithm. It can be seen that the corrected result of the proposed algorithm is better than those of Hough and Randon.

To verify the applicability of the proposed algorithm, Figure 11(a) of different resolutions, sizes and application scenarios are selected for experiment in the proposed algorithm. The experimental results are shown in Figure 11(b).

2. Experimental analysis

Since the corrected process of images in the proposed algorithm adopts the mapping principle of three-dimensional space. In Figures 8 and 9, it shows that when the mapping relation point E is not unique, it can float up and down on the Z-axis of three-dimensional space. Since several vertices of the image to be corrected are fixed, the size of the quadrilateral or triangle of the mapping result will change when the mapping relation point E floats up and down on the Z-axis of the three-dimensional space. When the corrected image is too large, the resolution of the image will be reduced.

Figure 12 shows the changing process of image deformation in the process of image enlargement. Part of the image pixels in Figure 12(a) are shown in Figure 12(b). When the image becomes larger, the image pixels are filled by the method of the bilinear interpolation in Figure 12(c), and the enlarged image is shown in Figure 12(d).

The size of Figure 13(b) corrected image is 0.75 times the size of the shooting image. The size of Figure 13

(a) (b)

Figure 11 Experimental results. (a) Shooting image; (b) The corrected result of the proposed algorithm.

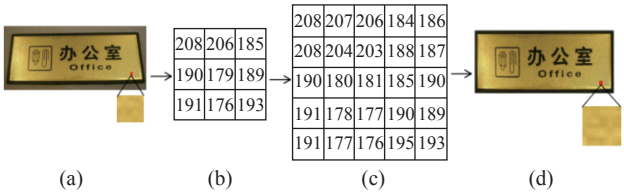

Figure 12 The principle of a change in the definition of an image. (a) Shooting image; (b) The pixels of the partially shooting image; (c) The pixel changes after the image is enlarged; (d) Magnified shooting image.

(c) corrected image is once the size of the shooting image. The size of Figure 13(d) corrected image is 1.5 times the size of the shooting image. From Figures 13(b), (c) and (d), the sizes of corrected images are different, the definition is different. The size of the corrected image used in the proposed algorithm is 0.9 times of the original quadrilateral background image and 1 time of the original triangular image.

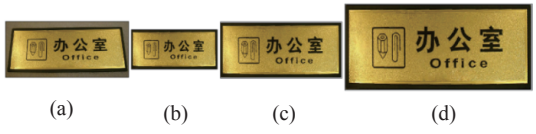

Figure 13 Comparison of corrected image size. (a) Shooting image; (b) Corrected result of 0.75 times; (c) Corrected result of 1 time; (d) Corrected result of 1.5 times.

3. Characteristics analysis of experimental result

As the images used in the experiments are sourced from the Internet, it is impossible to find the standard original image for comparison. In this paper, the correction results are measured from the edge and corner features of the corrected image, and the quantitative features are measured by the slope of the edge length of the corrected image, the interior angle, execution speed and the vertex displacement.

The experiment is carried out based on the image library of Matlab R2016b, and we test this algorithm using MATLAB on a laptop with a 3.6 GHz CPU and 8G RAM. In the proposed algorithm, a quadrilateral image and a triangular image are selected to compare the experimental results.

In (18) and (19), L_a represents the variance of the side length tilted angle and I_a represents the variance of the interior angle for the quadrilateral image, respectively. And T represents the running time. The experimental results are shown in Table 1.

$$L_a = \frac{(t_a - t_1)^2 + (t_b - t_2)^2 + (t_c - t_3)^2 + (t_d - t_4)^2}{4} \tag{18}$$

$$I_a = \frac{1}{n}\sum_{i=1}^{n=4}(t_i - t)^2 \tag{19}$$

where t_a, t_b, t_c and t_d respectively represent the slope of the left, top, right and bottom sides of the corrected quadrilateral image. t_1, t_2, t_3 and t_4 are the slope of the four sides of the standard rectangle, which respectively are 90°, 0°, 90° and 0°. t_i represents the degree of angles in the corrected quadrilateral image. t is the degrees inside the standard rectangle, which is 90°.

Table 1 Comparison of performance between different algorithms for quadrilateral image

Method	T (s)	L_a (deg^2)	I_a (deg^2)
Hough	**0.313**	1.6878	3.3756
Randon	0.569	1.2528	2.5055
The proposed algorithm	0.742	**0.2962**	**0.1754**

In (20) and (21), L_a represents the variance of the side length tilted angle and I_a represents the variance of the interior angle for the triangular image, respectively. And T represents the running time. The experimental results are shown in Table 2.

$$L_a = \frac{(t_a - t_1)^2 + (t_b - t_2)^2 + (t_c - t_3)^2}{3} \tag{20}$$

$$I_a = \frac{1}{n}\sum_{i=1}^{n=3}(t_i - t)^2 \tag{21}$$

where t_a, t_b and t_c respectively represent the slope of the left, right and bottom sides of the corrected triangular image. t_1, t_2 and t_3 are the slope of the three sides of the regular triangle, which respectively are 60°, 120° and 0°. t_i represents the degree of angles in the corrected triangular image. t is the degrees inside the regular triangle, which is 60°.

Table 2 Comparison of performance between different algorithms for triangular image

Method	T (s)	L_a (deg^2)	I_a (deg^2)
Hough	**0.313**	1.3136	3.3648
Randon	0.569	1.2223	3.3096
The proposed algorithm	1.138	**0.0281**	**0.0109**

As can be seen from Tables 1 and 2, although the proposed algorithm is slightly slower than the traditional Hough transform algorithm and Radon transform algorithm in terms of running time, the proposed algorithm is superior to the traditional Hough transform algorithm and Radon transform algorithm in terms of target image correction results.

The running time of the algorithm in the proposed algorithm varies with the size of the image. When the experimental image is larger, the running time of the algorithm in the proposed algorithm is longer; when the experimental image is smaller, the running time is shorter. This is because the proposed algorithm maps each pixel value of the target image. When the image to be corrected is larger, the numbers of pixels contained in the image and the pixel value of the pixels to be mapped are more, the longer the algorithm's running time will be.

We select 100 quadrilateral images and 100 triangular images for experiments respectively. Starting from the dimensions of execution time, length of side and angle of inclination in the corrected images, and interior angle in the length of side after correction, the experimental results of Hough transform algorithm and Radon transform algorithm and the proposed algorithm are analyzed and compared, and error histograms are drawn. The experimental results are shown in Figures 14–16.

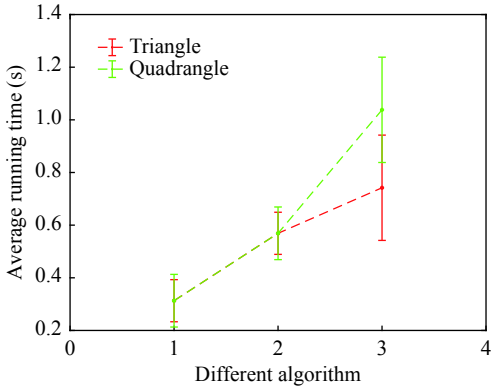

Figure 14 The mean-variance of the running time.

Figure 14 is a mean-variance graph of the running time for three different algorithms with triangle and rectangle targets respectively, where 1, 2 and 3 respectively represent the correction time by the algorithms of Hough, Randon and the proposed algorithm. The mean-variance graph shows the average of the distance from the average of each data, reflecting the dispersion of a data set. The larger the variance line, the larger the difference between most values and their average value. The smaller the error line, the closer these values are to the average, that is, the better the correction effect.

Figures 15(a) and (b) respectively show the mean variance of the four sides and four internal angles of the quadrilateral relative to the rectangle after correction of the triangle image by Hough, Randon and the proposed algorithm. Figure 16(a) and (b) respectively show the mean variance of the three sides and three internal angles of the triangle relative to the equilateral triangle after the correction of Hough, Randon and the proposed algorithm. It suggests that the corrected image by the proposed algorithm is closer to the standard rectangle and regular triangle. Through the comparative analysis of Figures 13–15, it concludes that although the proposed algorithm takes a longer time than the traditional algorithm, the corrected result is more robust than the traditional algorithm.

In addition, the proposed algorithm evaluates the recognition rate of 100 quadrilateral and 100 triangle images, as well as the mean displacement error (MDE) between the horizontal and vertical coordinates of the four corners and the real position of the four corners. The 200 images include 100 document images and 100 images of scene. Comparison of results of different algorithms

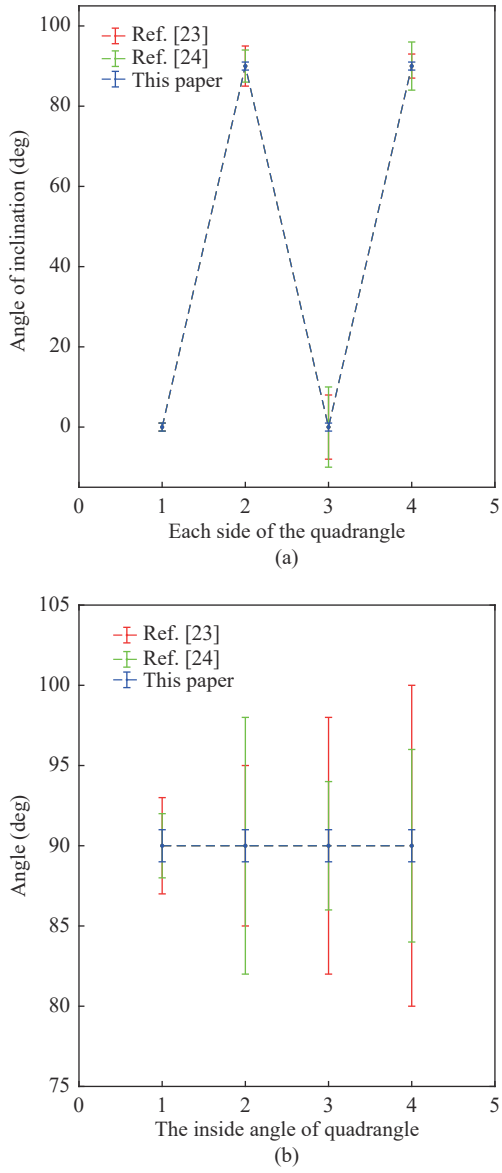

Figure 15 The mean-variance of quadrilateral. (a) The mean-variance of side's inclined plane; (b) The mean-variance of interior angle.

shown in Table 3. QS represents the success rate of the quadrilateral content, TS represents the success rate of the triangle content, QMDE represents the average displacement's error of the quadrilateral image, TMDE represents the average displacement's error of the triangle image. The MDE expression is shown in (22).

$$\mathrm{MDE} = \frac{1}{n}\sum_{i=1}^{n}\sum_{j=1}^{n}\left|y_p^{ij} - y^{ij}\right| \tag{22}$$

where $y^{ij}{}_p$ and y^{ij} respectively represent the coordinates of pixel points of the corrected image and the coordinates of original points, and n represents the number of angles of the polygon.

We made some distorted images manually and corrected them by this algorithm. The corrected results are shown in Figure 17.

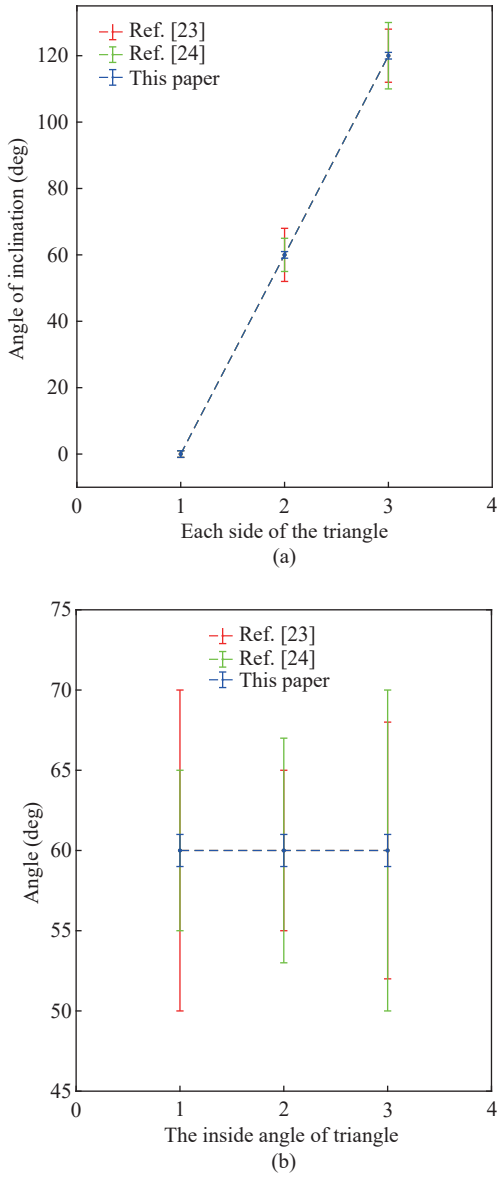

Figure 16 The mean-variance of triangle. (a) The mean-variance of side's inclined plane; (b) The mean-variance of interior angle.

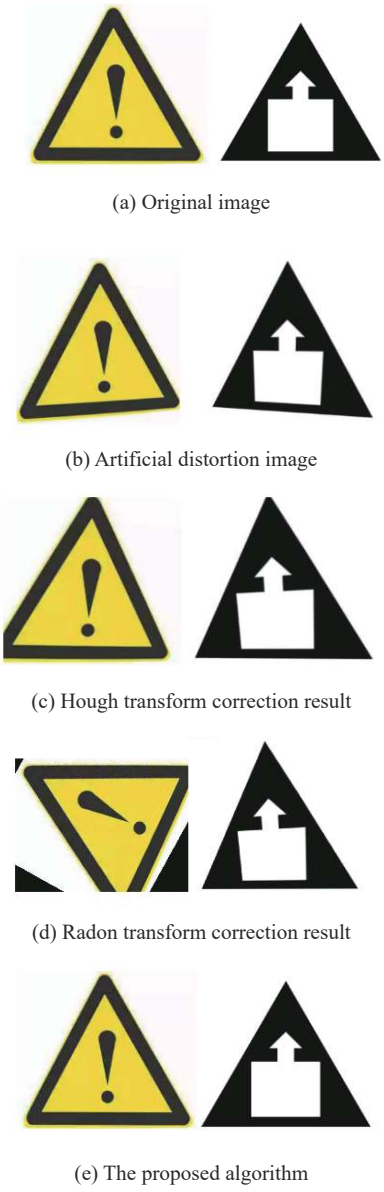

Figure 17 Experimental results.

Table 3 Comparison of corrected results between different algorithms

Method	QS	TS	QMDE	TMDE
Hough	83%	84%	961.76	838.04
Randon	81%	87%	824.08	741.21
[26]	89%	–	118.97	–
[28]	97%	–	981.73	–
[29]	–	–	75.57	–
The proposed algorithm	98%	99%	36.47	30.71

The correction results of the proposed algorithm are compared with those of Hough transform and Radon transform through the indexes of peak signal to noise ratio (PSNR), pixel accuracy (PA) and structural similarity (SSIM), and the comparison results are shown in Table 4. Tables 3 and 4 show that the proposed algorithm is more robust in the corrected results of deformity image in various scenes.

Table 4 Comparison of corrected results between different algorithms

Method	PSNR	PA	SSIM
Hough	33.3887	0.77	0.86
Radon	32.8731	0.81	0.88
The proposed algorithm	**39.9293**	**0.90**	**0.95**

IV. Conclusion

The adaptive image deformity correction algorithm proposed in this paper can solve the geometric deformation of the original image in geometric position, shape, size and orientation. Adaptive filtering, edge detection, mathematical morphology and connected domain filtering are used for initial experiments to enhance image edge attributes. Then the edge of the image is accurate-

ly determined by the combination of linear fitting and gradient ascent. In addition, in terms of data processing, for discrete points with large offsets in distribution, mean-square filtering method is adopted in the proposed algorithm to eliminate them, so as to reduce errors and prevent mutations from affecting the final image adjustment results. The geometric deformation image is projected into rectangular image by geometric center projection transformation. Finally, the effectiveness and feasibility of the improved algorithm are proved by simulation experiments and comparison with other algorithms. The disadvantage is that in the process of triangle image correction, due to the deformation of the image, it is impossible to determine whether the triangle image before the deformation is acute angle, right angle or obtuse angle. Since most triangle images in life are regular triangle images, the proposed algorithm defaults to regular triangle images after correction. In addition, the distortion correction of circular images and polygonal images has not been studied in this paper, which is what needs to be done in the next step of research.

Acknowledgements

This work was supported by the National Natural Science Foundation of China (Grant No. 61961037) and the Industrial Support Plan of Education Department of Gansu Province (Grant No. 2021CYZC-30).

References

[1] Z. L. Su, L. Lu, F. J. Yang, *et al.*, "Geometry constrained correlation adjustment for stereo reconstruction in 3D optical deformation measurements," *Optics Express*, vol. 28, no. 8, pp. 12219–12232, 2020.

[2] L. Ma, "Research on distance education image correction based on digital image processing technology," *EURASIP Journal on Image and Video Processing*, vol. 2019, no. 1, article no. 18, 2019.

[3] D. M. Feng, M. Q. Feng, E. Ozer, *et al.*, "A vision-based sensor for noncontact structural displacement measurement," *Sensors*, vol. 15, no. 7, pp. 16557–16575, 2015.

[4] M. Alipour, S. J. Washlesky, and D. K. Harris, "Field deployment and laboratory evaluation of 2D digital image correlation for deflection sensing in complex environments," *Journal of Bridge Engineering*, vol. 24, no. 4, article no. 04019010, 2019.

[5] W. Li, X. Zhang, and Z. R. Wang, "Music content authentication based on beat segmentation and fuzzy classification," *EURASIP Journal on Audio, Speech, and Music Processing*, vol. 2013, no. 1, article no. 11, 2013.

[6] R. A. Rakow-Penner, N. S. White, D. J. A. Margolis, *et al.*, "Prostate diffusion imaging with distortion correction," *Magnetic Resonance Imaging*, vol. 33, no. 9, pp. 1178–1181, 2015.

[7] B. Fu, H. Guo, X. L. Zhao, *et al.*, "Motion-blurred SIFT invariants based on sampling in image deformation space and univariate search," *IET Computer Vision*, vol. 10, no. 7, pp. 709–717, 2016.

[8] X. Y. Deng, Y. N. Zhang, and Y. H. Yang, "A shape recognition algorithm for traffic sign identification," *Computer Engineering and Science*, vol. 43, no. 2, pp. 322–328, 2021. (in Chinese)

[9] L. L. Li and H. B. Ma, "Pulse coupled neural network-based multimodal medical image fusion via guided filtering and WSEML in NSCT domain," *Entropy*, vol. 23, no. 5, article no. 591, 2021.

[10] Y. Mo, X. D. Kang, P. H. Duan, *et al.*, "Attribute filter based infrared and visible image fusion," *Information Fusion*, vol. 75, pp. 41–54, 2021.

[11] B. Meher, S. Agrawal, R. Panda, *et al.*, "A survey on region based image fusion methods," *Information Fusion*, vol. 48, pp. 119–132, 2019.

[12] B. Y. Liu, L. D. Wu, H. X. Hao, *et al.*, "Interferometric phase image denoising method via residual learning," *Journal of Electronic Imaging*, vol. 30, no. 2, article no. 023013, 2021.

[13] X. H. Yang, Y. Xu, Y. H. Quan, *et al.*, "Image denoising via sequential ensemble learning," *IEEE Transactions on Image Processing*, vol. 29, pp. 5038–5049, 2020.

[14] M. M. Mohammed, A. Badr, and M. B. Abdelhalim, "Image classification and retrieval using optimized pulse-coupled neural network," *Expert Systems with Applications*, vol. 42, no. 11, pp. 4927–4936, 2015.

[15] Y. C. Chen, F. Y. Huang, B. Q. Liu, *et al.*, "Significant obstacle location with ultra-wide FOV LWIR stereo vision system," *Optics and Lasers in Engineering*, vol. 129, article no. 106076, 2020.

[16] S. Zhang, B. Q. Liu, F. Y. Huang, *et al.*, "Super wide field of view staring infrared imaging technology and its application," *Laser & Infrared*, vol. 46, no. 10, pp. 1176–1182, 2016.

[17] S. W. Zhang, X. N. Zhang, Z. Y. Wu, *et al.*, "Research on asphalt mixture injury digital image based on enhancement and segmentation processing technology," *Applied Mechanics and Materials*, vol. 470, pp. 832–837, 2013.

[18] M. Lee, H. Kim, and J. Paik, "Correction of barrel distortion in fisheye lens images using image-based estimation of distortion parameters," *IEEE Access*, vol. 7, pp. 45723–45733, 2019.

[19] X. R. Mao, K. M. Liu, L. Y. Wang, *et al.*, "Image distortion correction algorithm based on FPGA," *Journal of Applied Optics*, vol. 41, no. 1, pp. 86–93, 2020. (in Chinese)

[20] K. Koolstra, T. O'Reilly, P. Börnert, *et al.*, "Image distortion correction for MRI in low field permanent magnet systems with strong B_0 inhomogeneity and gradient field nonlinearities," *Magnetic Resonance Materials in Physics, Biology and Medicine*, vol. 34, no. 4, pp. 631–642, 2021.

[21] Y. C. Chen, C. Deng, Y. Zhang, *et al.*, "Ultra-wide FOV infrared image distortion correction based on accurate model and back-projection," *Semiconductor Optoelectronics*, vol. 42, no. 4, pp. 546–550, 2021. (in Chinese)

[22] W. Guan, Z. L. Wang, Z. Q. Wang, *et al.*, "Precise axis centering calibration technology for optical lens," *Journal of Applied Optics*, vol. 39, no. 2, pp. 252–256, 2018. (in Chinese)

[23] S. S. Bafjaish, M. S. Azmi, M. N. Al-Mhiqani, *et al.*, "Skew detection and correction of Mushaf Al-Quran script using hough transform," *International Journal of Advanced Computer Science and Applications*, vol. 9, no. 8, pp. 402–409, 2018.

[24] M. Y. Yu, Q. G. Zhu, and Y. J. Wang, "Correction method of track image based on Canny operator and Radon transform," *Journal of Computer Applications*, vol. 37, no. S2, pp. 91–94,133, 2017. (in Chinese)

[25] L. Li, C. D. Tan, M. J. Liao, *et al.*, "Analytic reconstruction for parallel translational computed tomography based on radon inverse transform," *Acta Optica Sinica*, vol. 41, no. 6, article no. 0611003, 2021. (in Chinese)

[26] M. Li, Z. L. Su, and D. S. Zhang, "Methods for digital image correlation measurement with camera shake correction based on affine transformation," *Acta Optica Sinica*, vol. 41, no. 9, article no. 0912002, 2021. (in Chinese)

[27] X. J. Xu, X. F. Wang, W. Q. Lu, *et al.*, "Development of part contour recognition system based on edge detection," *Journal of Mechanical & Electrical Engineering*, vol. 36, no. 2, pp. 201–205, 2019. (in Chinese)

[28] K. Javed and F. Shafait, "Real-time document localization in natural images by recursive application of a CNN," in *Proceedings of the 14th IAPR International Conference on Document Analysis and Recognition (ICDAR)*, Kyoto, Japan, pp. 105–110, 2017.

[29] H. Yoo and K. Jun, "Deep corner prediction to rectify tilted license plate images," *Multimedia Systems*, vol. 27, no. 4, pp. 779–786, 2021.

[30] V. Abolhasannejad, X. M. Huang, and N. Namazi, "Developing an optical image-based method for bridge deformation measurement considering camera motion," *Sensors*, vol. 18, no. 9, article no. 2754, 2018.

[31] S. Yoneyama, A. Kitagawa, S. Iwata, *et al.*, "Bridge deflection measurement using digital image correlation," *Experimental Techniques*, vol. 31, no. 1, pp. 34–40, 2007.

[32] B. W. Jo, Y. S. Lee, J. H. Jo, *et al.*, "Computer vision-based bridge displacement measurements using rotation-invariant image processing technique," *Sustainability*, vol. 10, no. 6, article no. 1785, 2018.

[33] H. Y. Xu, X. L. Xu, and Y. B. Zuo, "Applying morphology to improve Canny operator's image segmentation method," *The Journal of Engineering*, vol. 2019, no. 23, pp. 8816–8819, 2019.

[34] S. J. Gong, G. Q. Li, Y. J. Zhang, *et al.*, "Application of static gesture segmentation based on an improved canny operator," *The Journal of Engineering*, vol. 2019, no. 15, pp. 543–546, 2019.

[35] X. Y. Deng, Y. H. Yang, H. Zhang, *et al.*, "PCNN double step firing mode for image edge detection," *Multimedia Tools and Applications*, vol. 81, no. 19, article no. pp. 27187–27213, 2022.

Xiangyu DENG was born in Gansu Province, China. He is currently a Professor with the College of Physics and Electronic Engineering, Northwest Normal University, Lanzhou, China. His current research interests include digital image processing, artificial neural networks, and pattern recognition.
(Email: dengxy000@126.com)

Aijia ZHANG was born in Hebei Province, China. She is currently an M.S. candidate with the School of Physics and Electronic Engineering, Northwest Normal University, Lanzhou, China. Her current research interest is digital image processing.
(Email: zaj_serendipity@126.com)

Jinhong YE was born in Guangzhou Province, China. He is currently an M.S. candidate with the School of Physics and Electronic Engineering, Northwest Normal University, Lanzhou, China. His current research interests are digital image processing and artificial intelligence.
(Email: yejh000@126.com)